CARBON 52 (2013) 379–387

Available at www.sciencedirect.com

SciVerse ScienceDirect

journal homepage: www.elsevier.com/locate/carbon

The transformation of a gold film on few-layer graphene to produce either hexagonal or triangular nanoparticles during annealing

Haiqing Zhou [a,b,c], *Fang Yu* [a,c], *Minjiang Chen* [a,c], *Caiyu Qiu* [b], *Huaichao Yang* [a,c], *Gang Wang* [a,c], *Ting Yu* [b,d,e], *Lianfeng Sun* [a,*]

[a] *National Center for Nanoscience and Technology, Beijing 100190, China*

[b] *Division of Physics and Applied Physics, School of Physical and Mathematical Sciences, Nanyang Technological University, Singapore 637371, Singapore*

[c] *Graduate School of Chinese Academy of Sciences, Beijing 100049, China*

[d] *Energy Research Institute at Nanyang Technological University (ERIAN), Singapore 639789, Singapore*

[e] *Department of Physics, Faculty of Science, National University of Singapore, Singapore 117542, Singapore*

ARTICLE INFO

Article history:
Received 8 August 2012
Accepted 22 September 2012
Available online 1 October 2012

ABSTRACT

The shape transformation of gold directly on graphene has been well studied by thermally annealing gold-deposited graphene samples at the temperature range from 600 to 800 °C. We find that few-layer graphene can be served as a platform to transform a gold film into mainly hexagonal gold nanoparticles (AuNPs) at 600 or 700 °C, or coexistence of hexagonal and triangular AuNPs at 800 °C. Especially, the size and density of these AuNPs are dependent on the number of graphene layers, indicating the strong relationship between gold shape transformation and the number of graphene layers on the substrate. We propose that annealing-induced growth of gold islands and the layer-dependent interactions among Au and *n*-layer graphene are the two main causes for this shape transformation. Meanwhile, Raman enhancing effects of these AuNPs are also investigated. These faceted AuNPs exhibit excellent SERS effects on Raman spectra of few-layer graphene with the enhancement factors up to several hundreds. Combined with *n*-layer graphenes, these faceted AuNPs can be used as graphene-based SERS substrates for increasing Raman signals of adsorbed rhodamine 6G molecules with a larger scale than those based on fresh graphenes.

1. Introduction

Due to the unique electronic properties and exceptionally high crystal quality, graphene has attracted great attention since it was firstly discovered in 2004 [1]. The exceptionally chemical and physical properties, such as high carrier mobility (200,000 $cm^2 V^{-1} s^{-1}$) [2], thermal conductivity (~5000 $Wm^{-1} K^{-1}$) [3–5], white light transmittance (~97.3%) [6], and large specific surface area (~2630 $m^2 g^{-1}$) [7], make graphene a promising candidate for potential applications in energy generation and storage, composites, and supercapacitors [8–14]. To attain this goal, chemical modification or functionalization of graphene can offer the effective approach to fabricate novel graphene-based composites or hybrids. Recently, various materials have been employed to synthesize graphene-based composites or hybrids, such as metal nanoparticles [15–22], boron nitride [23,24], metal oxides-based nanostructures [25,26], and multilayer graphene

* *Corresponding author:* Fax: +86 10 62656765.
E-mail address: slf@nanoctr.cn (L. Sun).

0008-6223/$ - see front matter
http://dx.doi.org/10.1016/j.carbon.2012.09.048

[27], etc. Beyond these materials, metal nanoparticles, especially gold nanoparticles (AuNPs) have been paid much attention because of their potential applications in catalysis, fuel cells, gas sensors and biological applications [16,28,29]. In order to attach metal nanoparticles onto the graphene surface, pre-modification of some organic spacers as the adhesives, like octadecylamine onto graphene surface is necessary. Following selective chemical functionalization, graphene oxides can be used as templates to tune the shape and crystalline of nanomaterials adsorbed on their surfaces [15,30,31]. However, on the basis of solution-phase, these chemical routes involve multistep chemical and physical processes as well as surfactants, solvent molecules, or unreacted chemical precursors. In the meantime, these chemical approaches and the presence of defects make graphite oxides very difficult to precisely control the shape of metal nanoparticles or investigate the excellent surface properties of graphene. Therefore, it is very attractive to introduce new physical methods to investigate the shape evolution of nanomaterials directly on *n*-layer graphenes without any chemical modification on graphene surface.

Although the interlayer interaction between graphene layers is very weak, *n*-layer graphenes exhibit excellent layer-dependent properties [6,32–35]. For example, with the increase of the number of graphene layers, the white light transmittance of suspended graphenes decreases linearly by a value of $\pi\alpha$, where $\alpha = e^2/hc \approx 1/137$ [6]. Also, after thermal evaporation of Ag or Au films onto graphenes, Raman scattering of *n*-layer graphenes is enhanced with a decreasing enhancement factor [32,33]. Moreover, the surface diffusion of gold on graphenes with different layer number is obviously different, which is attributed to different surface diffusion barriers of gold on *n*-layer graphenes [34] or different interactions among Au and graphenes [35]. Thus, as typically two-dimensional materials with mainly sp^2-bonded carbon sheets, *n*-layer graphenes can provide the ideal prototype to be effectively used as tunable substrates for controlling metal nanoparticles with different sizes and shapes because of their excellent layer-dependent surface properties [34,35].

In present work, we firstly report that few-layer graphene can be served as an extraordinary platform to tune a gold film into hexagonal or triangular AuNPs by means of thermal annealing with controlled temperature from 600 to 800 °C. Especially, with the increase of graphene thickness, the size of these AuNPs increases, while the particle density decreases. These results suggest that gold shape transformation is greatly related to the number of graphene layers. To understand the possible mechanisms, we propose that annealing-induced growth of gold islands and the interactions among Au and *n*-layer graphenes are the two main causes. The main advantage of performing this process is that surfactants, solvent molecules, or unreacted chemical precursors are absent, which can minimize the growth, dissolution, or severe reshaping of metal nanostructures. Meanwhile, these faceted AuNPs exhibit excellent surface-enhanced Raman scattering (SERS) properties, which can enhance Raman peak intensities of the characteristic G and 2D bands in graphene with two orders of magnitude larger than those collected on pristine *n*-layer graphenes by simply comparing the enhanced Raman signal with the normal Raman signal at the same ambient conditions. Combined with *n*-layer graphenes, these faceted AuNPs can be used as graphene-based SERS substrates to enhance Raman signals of adsorbed rhodamine 6G (R_6G) molecules on them, which exhibit much more obvious Raman enhancing effects than that based on fresh *n*-layer graphenes.

2. Experimental

2.1. Sample preparation and identification

Pristine *n*-layer graphenes were mechanically exfoliated from natural graphite (Alfa Aesar), and then transferred onto the silicon substrate with a 300 nm SiO_2 layer. The combined techniques of optical microscope (Leica DM 4000) and micro-Raman spectroscopy (Renishaw inVia Raman Spectroscope) were applied to determine the number of graphene layers.

2.2. Gold film deposition and thermal annealing

After thickness determination of *n*-layer graphenes, thin gold film was thermally deposited onto the silicon substrate-supported graphenes in a vacuum thermal evaporator at a deposition rate of 1.0 Å/s under a vacuum of $\sim 10^{-4}$ Pa. Then the gold-deposited graphene samples were thermally annealed in a quart tube, in the center of a tubular furnace at the temperatures above 600 °C and below 900 °C. During thermal annealing for about 2 h, a gas coflow of 200 sccm Ar and 10 sccm H_2 was introduced into the tubular furnace. At each step, all the samples were characterized by scanning electron microscopy (SEM) and Raman spectroscopy.

2.3. Micro-Raman spectroscopy

The micro-Raman spectroscopy (Renishaw inVia Raman Spectroscope) experiments were carried out under ambient conditions with 514.5 nm (2.41 eV) and 633 nm (1.96 eV) excitations. 514.5 nm laser excitation was used to determine the number of graphene layers, and to study Raman enhancements of well-faceted AuNPs/graphene hybrids on adsorbed R_6G molecules, while the SERS effects of well-faceted AuNPs on Raman spectra of *n*-layer graphenes were examined by 633 nm. In order to avoid laser induced heating on samples [36,37], the laser power was set below 1.0 mW. The application of a 100× objective lens with a numerical aperture of 0.90 can provide us a ~1 μm laser spot size. Many Raman spectra (~10) of pristine or Au-decorated graphenes were collected to ensure the credibility and repeatability of the results.

3. Results and discussion

The diagram designed for the experiments is shown in Fig. 1. After the thickness of *n*-layer graphenes was definitely determined [34], a thin gold film was thermally evaporated onto *n*-layer graphenes (Fig. 1a and Fig. S1, Supplementary material). Then the samples were submitted to a tube furnace for further thermal annealing in hydrogen and argon gas coflow (200 sccm/10 sccm, respectively) at the atmospheric pressure.

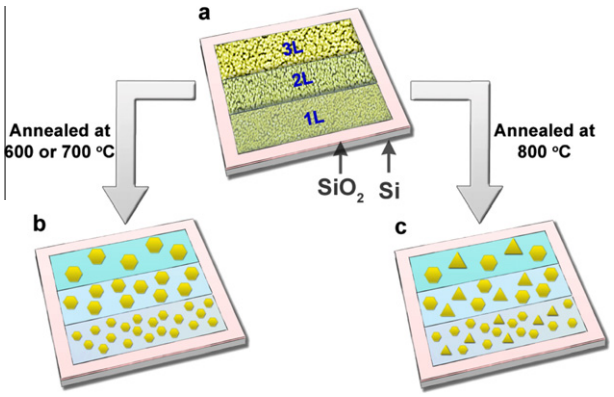

Fig. 1 – The diagram showing the annealing-induced gold shape transformation on graphenes at different annealing temperatures. (a) Thermal evaporation of gold film onto *n*-layer graphenes. (b) Hexagonal AuNPs formed on graphenes after annealing at 600 or 700 °C. (c) Coexistence of hexagonal and triangular AuNPs formed on graphenes after annealing at 800 °C.

After thermal annealing for about 2 h, the following results have been observed: firstly, if the annealing temperature is around 600 or 700 °C, gold film on *n*-layer graphenes can be tuned into hexagon-shaped AuNPs (Fig. 1b and Fig. S2, Supplementary material). Secondly, coexistence of hexagonal and triangular AuNPs on graphenes can be found after the samples annealed at 800 °C or a little above (Fig. 1c). Thirdly, the AuNPs exhibit almost irregular shape on graphenes when the temperature is around 900 °C (Fig. S3, Supplementary material). Moreover, the density and size of well-faceted AuNPs on *n*-layer graphenes are greatly related to the number of graphene layers. With the increase of graphene thickness, the particle size increases, while the particle density decreases. Finally, the well-faceted AuNPs can enhance Raman signals of graphenes with larger enhancement factors than that of gold film, indicating their potential applications as excellent graphene-based substrates for enhancing Raman signals of adsorbed molecules.

One of the interesting investigations here is that annealing-induced gold shape transformation is greatly related to the annealing temperature. With the temperature increases from 600 to 900 °C, gold films on graphenes have gradually evolved into hexagon-shaped AuNPs at 600 or 700 °C, coexistent hexagonal and triangular AuNPs at 800 °C, and irregular-shaped AuNPs at 900 °C. For example, after thermal annealing at 600 or 700 °C, we can find that gold film has been transformed into hexagon-shaped AuNPs as shown in Fig. 2 and Fig. S2 (Supplementary material). Also, the average particle size and density are highly determined by the number of graphene layers. With the increase of the layer number, the size of hexagonal AuNPs increases, while the particle density decreases, indicating that *n*-layer graphene ($n = 1, 2, 3, 4$) play an important role in this gold shape transformation.

Meanwhile, when the annealing temperature increases to 800 °C, hexagonal and triangular AuNPs coexist on the surface of *n*-layer graphenes as displayed in Fig. 3, which also exhibit thickness-dependent behaviors. Similar to that at 700 °C, with the increase of graphene thickness, the particle size also increases, while the particle density decreases, indicating that graphene-modulated gold shape transformation is greatly related to the layer number of *n*-layer graphenes.

To well account for this gold shape transformation, the following two main factors should be considered. On one hand, it is theoretically predicted that gold adatoms are weakly bonded with carbon atoms on graphene surface. This bonding can be viewed as physical adsorption, rather than chemical bonding, which is greatly related to the number of graphene layers [34,35,38–40]. With the increase of layer number "*n*", due to the weak inter-layer interaction, the interaction between gold adatoms and *n*-layer graphene ($n = 1, 2, 3, 4$) becomes much weaker, resulting in the thickness-dependent particle size and density of AuNPs on graphenes. Therefore, different interactions among gold and *n*-layer graphenes play a significant role in gold surface diffusion and shape transformation based on these two discussions: Firstly, as shown in Figs. 2 and 3, almost all the gold films have been transformed into AuNPs with faceted shapes on *n*-layer graphenes. Secondly, it is obvious to find that the size of faceted AuNPs exhibits layer-dependent behaviors, which is well consistent with recently reported thickness-dependent morphologies of gold and silver on graphenes [34,35,41]. As is reported, surface diffusion of metal adatoms on graphenes can be described by these two equations [34,41,42]: $D \propto \exp(-E_n/KT)$, $N \propto (1/D)^{1/3}$. Thus, we can obtain the particle density $N \propto \exp(E_n/3KT)$, where K is the Boltzmann constant, E_n is surface diffusion barrier of graphenes, D is the surface diffusion coefficient, and T the temperature. According to the observed thickness-dependent behaviors in Figs. 2 and 3, we can conclude that the decrease of surface diffusion barrier with layer number increasing is applicable here to explain the thickness-dependent shape transformation of gold on *n*-layer graphenes. On the other hand, annealing-induced gold diffusion or evaporation [43] is also very important in this gold shape transformation. According to these SEM images shown in Figs. 2 and 3, we can find that gold-covered regions on the surface of *n*-layer graphenes are all reduced. The decrease in gold-covered areas is mainly related to the enlarging growth of gold islands as well as gold evaporation from graphene surface during thermal annealing. Considering that the annealing temperature employed here is in the range between 600 °C and 800 °C, which is far below the melting temperature of bulk gold (~1064 °C), thermal annealing process mainly results in gold cluster diffusion and diffusion of gold atoms on graphene surface, rather than thermal evaporation of gold apart from graphene surface. That is, the nearby gold clusters tend to migrate along the surrounding larger clusters until they integrate into the largest Au domains, while atomic diffusion takes place for smaller Au clusters located far away from the larger clusters [43]. However, in these cases, we should take the interactions among *n*-layer graphenes and gold adatoms, and gold film thickness into consideration. The different interactions among graphenes and gold can be well understood from layer-dependent particle size and density shown in Figs. 2 and 3, while the influence of gold film thickness [15] on this shape transformation is confirmed by the following Fig. 4. Therefore, to search for the possible origin on the formation of well-faceted AuNPs on graphenes,

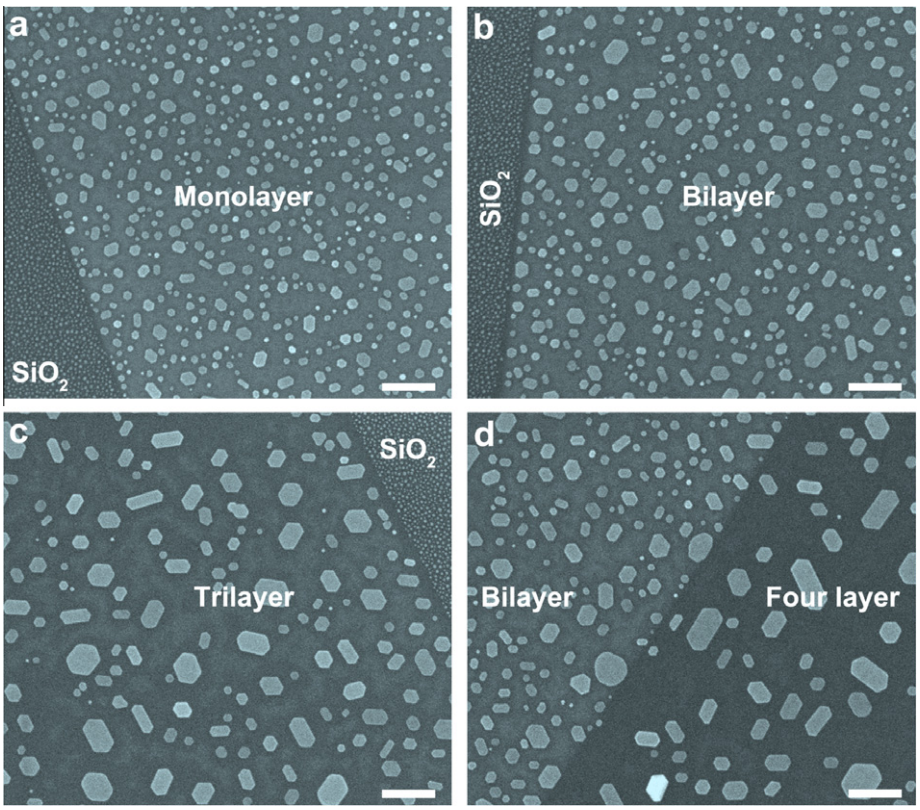

Fig. 2 – SEM images showing the transformation of gold films into hexagonal AuNPs on graphenes after thermal annealing at 700 °C for 2 h. Film thickness: 2.0 nm. Scale bar: 200 nm. (a) Hexagonal AuNPs on SiO_2 (left) and monolayer graphene (right). (b) Hexagonal AuNPs on SiO_2 (left) and bilayer graphene (right). (c) Hexagonal AuNPs on trilayer graphene (left) and SiO_2 (right). (d) Hexagonal AuNPs on bilayer (left) and four layer graphene (right). It is obviously observable that the size and density of hexagonal AuNPs depend on the number of graphene layers.

annealing-induced growth of gold islands and different surface properties of *n*-layer graphenes are the two main causes of the observed gold shape transformation on graphenes.

The second important investigation is that graphene-tuned gold shape transformation can be affected by gold film thickness, which is shown in Fig. 4. Fig. 4a and b correspond to gold shape transformation of 1.0 nm gold film deposited onto graphenes after thermal annealing at 600 °C, Fig. 4c and d are corresponding to 1.5 nm gold film after thermal annealing at 600 °C, and Fig. 4e and f stand for the annealing-induced shape transformation of 2.0 nm gold film at 600 °C.

With the increase of gold film thickness, the modulation of graphene on the shape of AuNPs becomes less and less distinct. When film thickness is below 2.0 nm, after thermal annealing at 600 or 700 °C, almost all the AuNPs show hexagonal shape. Whereas for 5.0 nm gold film or more (Fig. S4, Supplementary material), although hexagon-shaped AuNPs still exist after annealing at 600 °C, the AuNPs are not well faceted, indicating that gold film thickness has great effects on annealing-induced gold shape transformation. That is to say, when gold film thickness is at ultra-small dimensions (for example, less than 5 nm), *n*-layer graphenes can be used as templates to tune gold film into hexagon-shaped AuNPs with the assistance of thermal annealing. For gold film much thicker than 5 nm, such as 15 nm, almost all the AuNPs become irregular nanoparticles with no faceted shapes, which can be well figured out in Fig. S5 (Supplementary material). Also, film thickness-related effects can be clearly observed when comparing the AuNPs on multilayer graphene or graphite (Fig. S6, Supplementary material).

Again, it is interesting to note that compared with 2 nm gold film on graphenes, the faceted AuNPs on graphenes exhibit very excellent SERS effects, which can enhance Raman signals of *n*-layer graphenes with larger Raman enhancement factors as shown in Fig. 5 and Table S1 (Supplementary material). As is reported, the enhancement strength on Raman scattering of *n*-layer graphenes is observed to depend on the excitation wavelength [32], in which almost no Raman enhancing effects have been found for gold on graphene at 514 nm laser excitation, while Raman scattering of *n*-layer graphenes is greatly enhanced by gold deposition using 633 nm laser excitation. These observations have been also systematically discussed in our previous work by depositing different kind of metal species onto graphene [41]. Therefore, to well present Raman enhancing effects of these faceted AuNPs on Raman spectra of graphene, 633 nm laser excitation is selected in present work. As shown in Fig. 5a and b, although 2 nm gold film deposition can result in Raman enhancing effects on Raman spectra of *n*-layer graphenes, the corresponding enhancement factor is very small (Table S1, Supplementary material). However, after thermal

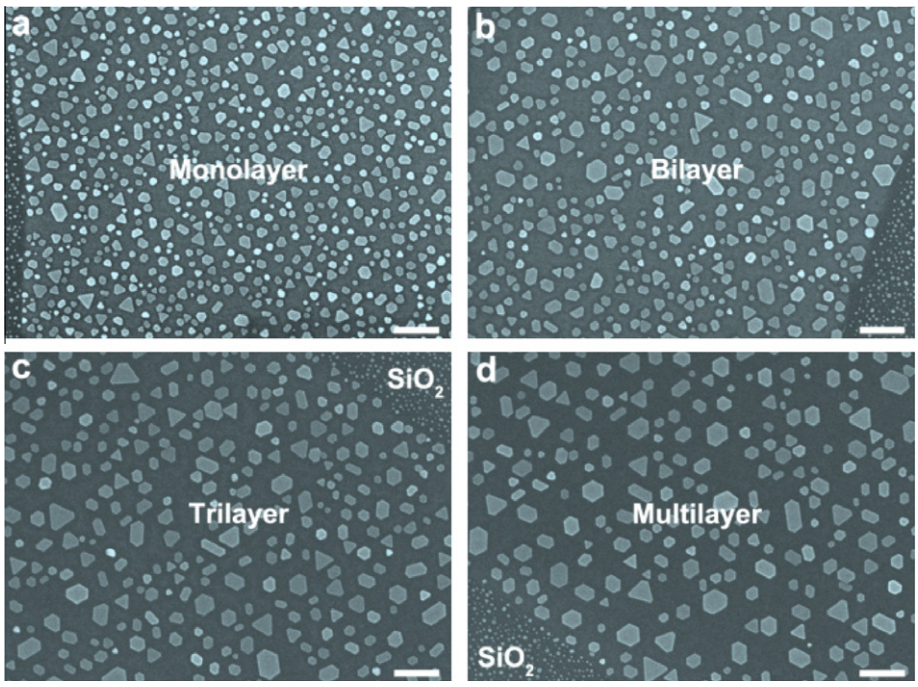

Fig. 3 – The coexistence of hexagonal and triangular AuNPs after thermal annealing at 800 °C for about 2 h. Film thickness: 2.0 nm. Scale bar: 200 nm. (a) AuNPs on SiO_2 (left) and monolayer graphene (right). (b) AuNPs on bilayer graphene (left) and SiO_2 (right). (c) AuNPs on trilayer graphene (left) and SiO_2 (right). (d) AuNPs on SiO_2 (left) and multilayer graphene (right). The size and density of hexagonal or triangular AuNPs on *n*-layer graphenes are still greatly related to the number of graphene layers.

annealing at 700 °C, the obtained hexagonal AuNPs can greatly enhance Raman signals of graphenes up to two orders of magnitude. Also, after thermal annealing at 800 °C, Raman scattering of monolayer and bilayer graphene can be enhanced with a larger enhancement factor than that by gold film, which is shown in Fig. 5c and d. For example, as is summarized in Table S1 in the Supplementary material, for 2 nm gold film, the enhancement factor is 10.2 for G peak of monolayer graphene. Noticeably, after thermal annealing at 700 or 800 °C, the enhancement factor of G peak is increased to 139.4 or 225.0, which is about several ten times larger than that by gold film. These investigations indicate that these faceted AuNPs can be potentially applied as graphene-based substrates to detect the adsorbed molecules with improved Raman enhancement.

More noticeably, as shown in Fig. 5, compared with that of pristine *n*-layer graphenes (black-marked), Raman peak intensities of monolayer and bilayer graphene are greatly enhanced by well-faceted AuNPs, and the enhancement factors of the characteristic Raman peaks, such as G and 2D peaks appear to be about two orders of magnitude. This value is much larger than recently reported results about Ag and Au on graphenes [32,33,41]. To well account for these improved Raman enhancing effects, it is necessary for us to consider the plasma resonance in AuNPs, which is highly sensitive to the subtle difference in their shape and size. Thus, these SERS spectra (Fig. 5) can be viewed as a perfect and indirect demonstration of improved SERS efficiency for faceted AuNPs on graphenes, suggesting that these faceted AuNPs can be potentially applied as excellent graphene-based substrates for enhancing Raman signals of adsorbed molecules [44–46].

It is well-known that the surface plasmon resonance and SERS enhancement of AuNPs critically depend on the size, size distribution, shape and surface state [47,48]. Although the spherical nanoparticles sometimes exhibit better Raman enhancements than plate-like ones, it is interesting for us to investigate the SERS effects of hexagonal or triangular AuNPs on adsorbed molecules, since these faceted AuNPs exhibit some different properties from spherical AuNPs due to their anisotropic shape. Compared with the spherical AuNPs, these hexagonal AuNPs have atomically smooth surfaces with sharp corners and edges, and they are highly crystallized single crystals with a preferential growth direction along the gold {111} facets, indicating their potential use as a tip-enhanced Raman scattering (TERS) substrate for TERS measurements [49,50]. Also, the ratio of surface to bulk atoms of plate-like nanoparticles is much higher than that of spherical ones, so the so-called broad but weak quadrupole plasmon modes are present in the near-infrared (near-IR) region of 700–2000 nm for gold nanoplates rather than spherical AuNPs, which reflects the anisotropic nature of gold nanoplates [51,52]. These unique optical properties enables the use of these metallic nanostructures to be designed for potentially high SERS enhancements of biomolecules using near-infrared laser excitations. Therefore, due to their well-defined surfaces, sharp corners and unusual optical properties, these faceted AuNPs can be served as ideal SERS substrates for studying the SERS activities in many fields.

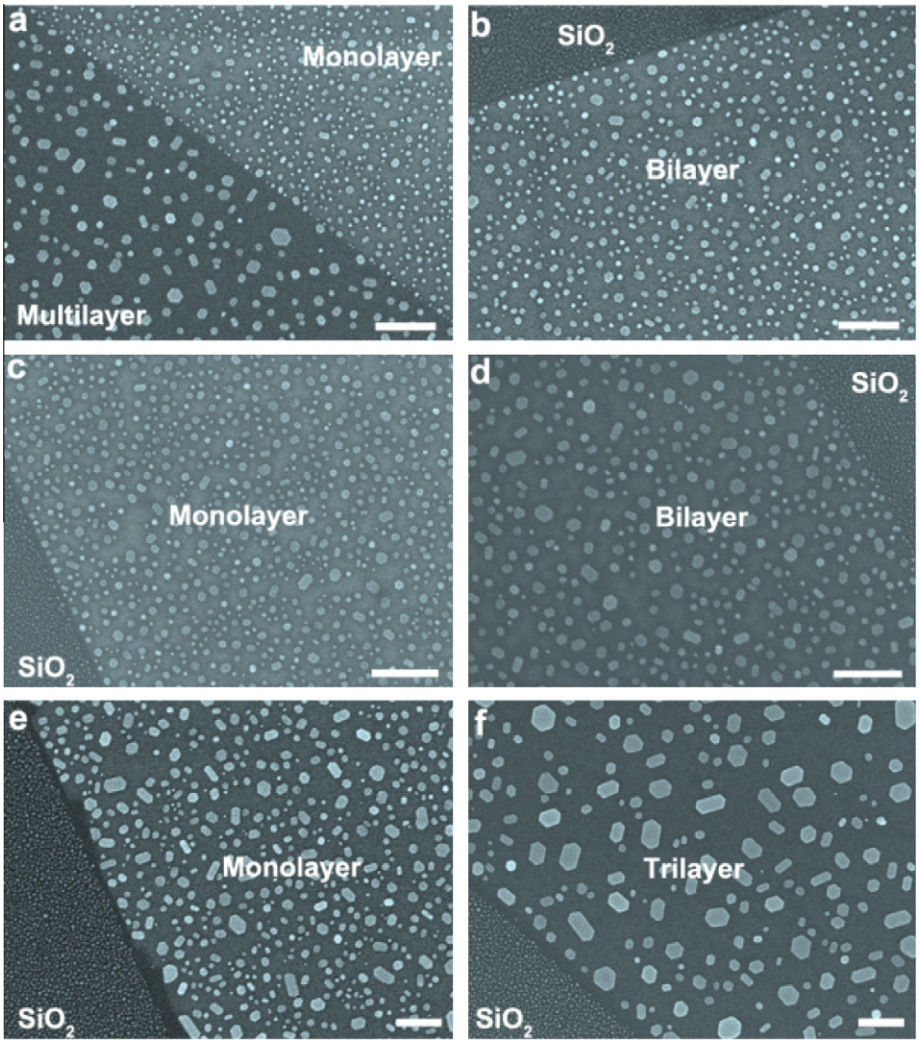

Fig. 4 – The effects of gold film thickness on graphene-tuned gold shape transformation after thermal annealing at 600 °C for 2 h. Scale bar: 200 nm. (a and b) 1.0 nm. (c and d) 1.5 nm. (e and f) 2.0 nm. It is obvious to find that with the increase of gold film thickness, the modulation becomes less effective.

The Raman enhancing effects of faceted AuNPs/graphene hybrids on adsorbed R_6G molecules have been investigated, which are shown Fig. 6. For comparison, Raman signals of R_6G molecules adsorbed on the surfaces of fresh *n*-layer graphenes are also displayed. All the spectra shown here were collected under the same ambient conditions (laser power, exposure time, etc.). In these Raman spectra, the prominent Raman peaks (~611.9, 773.5, 1185.4, 1310.9, 1361.7, 1506.6, 1574.9, and 1649.6 cm^{-1}) are attributed to the Raman peaks unique to R_6G molecules, while the Raman peak at around 1598.5 cm^{-1} is from graphene. Compared with fresh monolayer or bilayer graphene (black-marked), it is obvious to find that almost all the Raman peak intensities become much stronger for R_6G molecules on hexagonal AuNPs/graphene hybrids (red-marked), or combined hexagonal and triangular AuNPs/graphene hybrids (blue-marked), meaning that these faceted AuNPs can be applied to improve the Raman efficiency of *n*-layer graphenes served as SERS substrates. Therefore, the combination of well-faceted AuNPs and *n*-layer graphenes can be used as improved SERS substrates for enhancing Raman signals of adsorbed molecules with very low concentration [53–55].

4. Conclusions

We report that few-layer graphene can be used as a template for the transformation of a gold film into either hexagonal or triangular AuNPs by thermal annealing at a controlled temperature from 600 to 800 °C. After thermal annealing at the temperatures lower than the melting temperature of bulk gold (~1064 °C), the gold film on graphenes tends to reconstruct into hexagonal AuNPs at 600 or 700 °C, or coexistence of hexagonal and triangular AuNPs at 800 °C. These faceted AuNPs can exhibit excellent SERS effects on Raman signals of the characteristic G and 2D peaks in few-layer graphene with two orders of magnitude times of the original states. Also, after the decoration of these faceted AuNPs, few-layer graphene exhibits much more obvious Raman enhancing effects on Raman signals of adsorbed molecules than that based on fresh *n*-layer graphenes. Therefore, these faceted

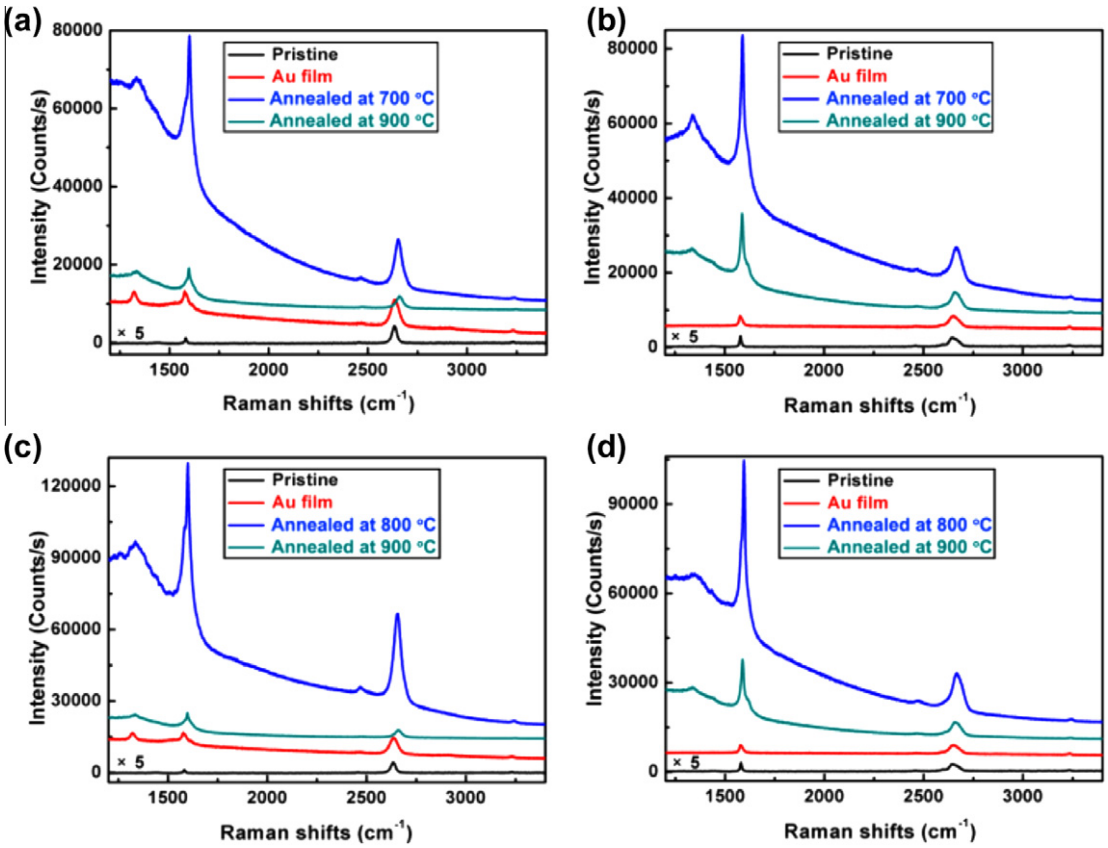

Fig. 5 – Highly-improved SERS efficiency of well-faceted AuNPs on *n*-layer graphenes excited by 633 nm at different annealing temperatures. (a) Monolayer and (b) bilayer graphene at 700 °C. (c) Monolayer and (d) bilayer graphene at 800 °C. It is clearly observable that compared with that enhanced by 2 nm gold film (red-marked) or spherical AuNPs (dark cyan-marked) after annealing at 900 °C, Raman scattering of *n*-layer graphenes is enhanced much more obviously by well-faceted AuNPs (blue-marked), indicating their highly-improved SERS efficiency. (For interpretation of the references to color in this figure legend, the reader is referred to the web version of this article.)

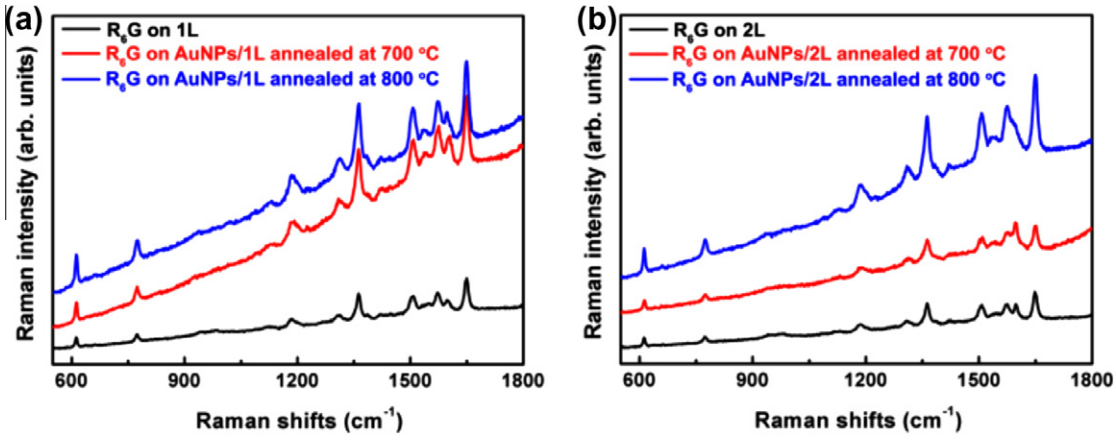

Fig. 6 – The comparison on the Raman enhancements of fresh and well-faceted AuNPs-decorated monolayer (a) and bilayer (b) graphene excited by 514.5 nm laser excitation. It is observable that after thermal annealing at 700 or 800 °C, the obtained well-faceted AuNPs can result in much more excellent Raman enhancing effects of *n*-layer graphenes on Raman signals of R_6G molecules (5 μM in water) than that based on fresh *n*-layer graphenes, indicating highly-improved Raman efficiency of graphene after the decoration of well-faceted AuNPs.

AuNPs on few-layer graphene can be potentially used in graphene-based SERS applications.

Acknowledgement

This work was supported by National Science Foundation of China (Grant Nos. 10774032, 90921001).

Appendix A. Supplementary data

Supplementary data associated with this article can be found, in the online version, at http://dx.doi.org/10.1016/j.carbon.2012.09.048.

REFERENCES

[1] Novoselov KS, Geim AK, Morozov SV, Jiang D, Zhang Y, Dubonos SV, et al. Electric field effect in atomically thin carbon films. Science 2004;306(5696):666–9.
[2] Du X, Skachko I, Barker A, Andrei E. Approaching ballistic transport in suspended graphene. Nat Nanotechnol 2008;3(8):491–5.
[3] Balandin AA, Ghosh S, Bao W, Calizo I, Teweldebrhan D, Miao F, et al. Superior thermal conductivity of single-layer graphene. Nano Lett 2008;8(3):902–7.
[4] Balandin AA. Thermal properties of graphene and nanostructured carbon materials. Nat Mater 2011;10(8):569–81.
[5] Nika DL, Balandin AA. Two-dimensional phonon transport in graphene. J Phys: Condens Matter 2012;24(23):233203.
[6] Nair RR, Blake P, Grigorenko AN, Novoselov KS, Booth TJ, Stauber T, et al. Fine structure constant defines visual transparency of graphene. Science 2008;320(5881):1308.
[7] Stoller MD, Park S, Zhu Y, An J, Ruoff RS. Graphene-based ultracapacitors. Nano Lett 2008;8(10):3498–502.
[8] Huang X, Qi XY, Boey F, Zhang H. Graphene-based composites. Chem Soc Rev 2012;41(2):666–86.
[9] Gilje S, Han S, Wang MS, Wang KL, Kaner RB. A chemical route to graphene for device applications. Nano Lett 2007;7(11):3394–8.
[10] Rafiee MA, Lu W, Thomas AV, Zandiatashbar A, Rafiee J, Tour JM, et al. Graphene nanoribbon composites. ACS Nano 2010;4(12):7415–20.
[11] Yin ZY, Wu SX, Zhou XZ, Huang X, Zhang QC, Boey F, et al. Electrochemical deposition of ZnO nanorods on transparent reduced graphene oxide electrodes for hybrid dolar vells. Small 2010;6(2):307–12.
[12] Huang X, Yin ZY, Wu SX, Qi XY, He QY, Zhang QC, et al. Graphene-based materials: synthesis, characterization, properties, and applications. Small 2011;7(14):1876–902.
[13] Cao XH, Shi YM, Shi WH, Lu G, Huang X, Yan QY, et al. Preparation of novel 3D graphene networks for supercapacitor applications. Small 2011;7(22):3163–8.
[14] Qi XY, Li H, Lam JWY, Yuan XT, Wei J, Tang BZ, et al. Graphene oxide as a novel nanoplatform for enhancement of aggregation-induced emission of silole fluorophores. Adv Mater 2012;24(30):4191–5.
[15] Huang X, Li SZ, Huang YZ, Wu SX, Zhou XZ, Li SZ, et al. Synthesis of hexagonal close-packed gold nanostructures. Nat Commun 2011;2:292.
[16] Johnson JL, Behnam A, Pearton SJ, Ural A. Hydrogen sensing using Pd-functionalized multi-layer graphene nanoribbon networks. Adv Mater 2010;22(43):4877–80.
[17] Jin Z, Nackashi D, Lu W, Kittrell C, Tour JM. Decoration, migration, and aggregation of palladium nanoparticles on graphene sheets. Chem Mater 2010;22(20):5695–9.
[18] Sidorov AN, Sławiński GW, Jayatissa AH, Zamborini FP, Sumanasekera GU. A surface-enhanced Raman spectroscopy study of thin graphene sheets functionalized with gold and silver nanostructures by seed-mediated growth. Carbon 2012;50(2):699–705.
[19] Huang X, Zhou XZ, Wu SX, Wei YY, Qi XY, Zhang J, et al. Reduced graphene oxide-templated photochemical synthesis and in situ assembly of Au nanodots to orderly patterned Au nanodot chains. Small 2010;6(4):513–6.
[20] Huang X, Li H, Li SZ, Wu SX, Boey F, Ma J, et al. Synthesis of gold square-like plates from ultrathin gold square sheets: the evolution of structure phase and shape. Angew Chem Int Ed 2011;50(51):12245–8.
[21] Huang X, Li SZ, Wu SX, Huang YZ, Boey F, Gan CL, et al. Graphene oxide-templated synthesis of ultrathin or tadpole-shaped Au nanowires with alternating hcp and fcc domains. Adv Mater 2012;24(7):979–83.
[22] Goyal V, Balandin AA. Thermal properties of the hybrid graphene-metal nano-micro-composites: applications in thermal interface materials. Appl Phys Lett 2012;100(7):073113.
[23] Ci LJ, Song L, Jin CH, Jariwala D, Wu DX, Li YJ, et al. Atomic layers of hybridized boron nitride and graphene domains. Nat Mater 2010;9(5):430–5.
[24] Liu Z, Song L, Zhao SZ, Huang JQ, Ma LL, Zhang JN, et al. Direct growth of graphene/hexagonal boron nitride stacked layers. Nano Lett 2011;11(5):2032–7.
[25] Yu DS, Nagelli E, Naik R, Dai LM. Asymmetrically functionalized graphene for photodependent diode rectifying behavior. Angew Chem Int Ed 2011;50(29):6575–8.
[26] Lin J, Penchev M, Wang GP, Paul RK, Zhong JB, Jing XY, et al. Heterogeneous graphene nanostructures: ZnO nanostructures grown on large-area graphene layers. Small 2010;6(21):2448–52.
[27] Shahil KMF, Balandin AA. Graphene-multilayer graphene nanocomposites as highly efficient thermal interface materials. Nano Lett 2012;12(2):861–7.
[28] Schedin F, Geim AK, Morozov SV, Hill EW, Blake P, Katsnelson MI, et al. Detection of individual gas molecules adsorbed on graphene. Nat Mater 2007;6(9):652–5.
[29] Wang ZJ, Zhang J, Yin ZY, Wu SX, Mandler D, Zhang H. Fabrication of nanoelectrode ensembles by electrodepositon of Au nanoparticles on single-layer graphene oxide sheets. Nanoscale 2012;4(8):2728–33.
[30] Huang X, Qi XY, Huang YZ, Li SZ, Xue C, Gan CL, et al. Photochemically controlled synthesis of anisotropic Au nanostructures: platelet-like Au nanorods and six-star Au nanoparticles. ACS Nano 2010;4(10):6196–202.
[31] Li YG, Wang HL, Xie LM, Liang YY, Hong GS, Dai HJ. MoS_2 nanoparticles grown on graphene: an advanced catalyst for the hydrogen evolution reaction. J Am Chem Soc 2011;133(19):7296–9.
[32] Lee J, Shim S, Kim B, Shin HS. Surface-enhanced Raman scattering of single- and few-layer graphene by the deposition of gold nanoparticles. Chem Eur J 2011;17(8):2381–7.
[33] Lee J, Novoselov KS, Shin HS. Interaction between metal and graphene: dependence on the layer number of graphene. ACS Nano 2011;5(1):608–12.
[34] Zhou HQ, Qiu CY, Liu Z, Yang HC, Hu LJ, Liu J, et al. Thickness-dependent morphologies of gold on *n*-layer graphenes. J Am Chem Soc 2010;132(3):944–6.
[35] Luo ZT, Somers LA, Dan YP, Ly T, Kybert NJ, Mele EJ, et al. Size-selective nanoparticle growth on few-layer graphene films. Nano Lett 2010;10(3):777–81.

[36] Calizo I, Balandin AA, Bao W, Miao F, Lau CN. Temperature dependence of the Raman spectra of graphene and graphene multilayers. Nano Lett 2007;7(9):2645–9.
[37] Calizo I, Bejenari I, Rahman M, Liu GX, Balandin AA. Ultraviolet Raman microscopy of single and multilayer graphene. J Appl Phys 2009;106(4):043509.
[38] Giovannetti G, Khomyakov PA, Brocks G, Karpan VM, van den Brink J, Kelly PJ. Doping graphene with metal contacts. Phys Rev Lett 2008;101(2):026803.
[39] Ling X, Zhang J. First-layer effect in graphene-enhanced Raman scattering. Small 2010;6(18):2020–5.
[40] Zhou HQ, Yu F, Yang HC, Qiu CY, Chen MJ, Hu LJ, et al. Layer-dependent morphologies and charge transfer of Pd on *n*-layer graphenes. Chem Commun 2011;47(33):9408–10.
[41] Zhou HQ, Qiu CY, Yu F, Yang HC, Chen MJ, Hu LJ, et al. Thickness-dependent morphologies and surface-enhanced Raman scattering of Ag deposited on *n*-layer graphenes. J Phys Chem C 2011;115(23):11348–54.
[42] Ma LY, Tang L, Guan ZL, He K, An K, Ma XC, et al. Quantum size effect on adatom surface diffusion. Phys Rev Lett 2006;97(26):266102.
[43] Figuerola A, Huis M, Zanella M, Genovese A, Marras S, Falqui A, et al. Epitaxial CdSe-Au nanocrystal heterostructures by thermal annealing. Nano Lett 2010;10(8):3028–36.
[44] Xu C, Wang X. Fabrication of flexible metal-nanoparticte film using graphene oxide sheets as substrate. Small 2009;5(19):2212–7.
[45] Ling X, Xie LM, Fang Y, Xu H, Zhang HL, Kong J, et al. Can graphene be used as a substrate for Raman enhancement? Nano Lett 2010;10(2):553–61.
[46] Xie LM, Ling X, Fang Y, Zhang J, Liu ZF. Graphene as a substrate to suppress fluorescence in resonance Raman spectroscopy. J Am Chem Soc 2009;131(29):9890–1.
[47] Ko H, Singamaneni S, Tsukruk VV. Nanostructured surfaces and assemblies as SERS media. Small 2008;4(10):1576–99.
[48] Zhang JT, Li XL, Sun XM, Li YD. Surface enhanced Raman scattering effects of silver colloids with different shapes. J Phys Chem B 2005;109(25):12544–8.
[49] Ren B, Gennaro P, Bruno P, Rolf S, Gerhard E. Tip-enhanced Raman spectroscopy of benzenethiol adsorbed on Au and Pt single-crystal surfaces. Angew Chem Int Ed 2005;44(1):139–42.
[50] Pienpinijtham P, Han XX, Suzuki T, Thammacharoen C, Ekgasit S, Ozaki Y. Micrometer-sized gold nanoplates: starch-mediated photochemical reduction synthesis and possibility of application to tip-enhanced Raman scattering (TERS). Phys Chem Chem Phys 2012;14:9636–41.
[51] Sun XP, Dong SJ, Wang EK. Large-scale synthesis of micrometer-scale single-crystalline Au plates of nanometer thickness by a wet-chemical route. Angew Chem Int Ed 2004;43(46):6360–3.
[52] Millstone JE, Park S, Shuford KL, Qin LD, Schatz GC, Mirkin CA. Observation of a quadrupole plasmon mode for a colloidal slution of gold nanoprisms. J Am Chem Soc 2005;127(15):5312–3.
[53] Wang YY, Ni ZH, Hu HL, Hao YF, Wong CP, Yu T, et al. Gold on graphene as a substrate for surface enhanced Raman scattering study. Appl Phys Lett 2010;97(16):163111.
[54] Fu XQ, Bei FL, Wang X, O'Brien S, Lombardi JR. Excitation profile of surface-enhanced Raman scattering in graphene-metal nanoparticle based derivatives. Nanoscale 2010;2(8):1461–6.
[55] Yu XX, Lin K, Qiu KQ, Cai HB, Li XJ, Liu JY, et al. Increased chemical enhancement of Raman spectra for molecules adsorbed on fluorinated reduced graphene oxide. Carbon 2012;50(12):4512–7.